In-Situ *X-Ray Diffraction Observations of Low-Temperature Ag-Nanoink Sintering and High-Temperature Eutectic Reaction with Copper*

John W. Elmer & E. D. Specht

Metallurgical and Materials Transactions A

ISSN 1073-5623
Volume 43
Number 5

Metall and Mat Trans A (2012)
43:1528-1537
DOI 10.1007/s11661-011-0717-9

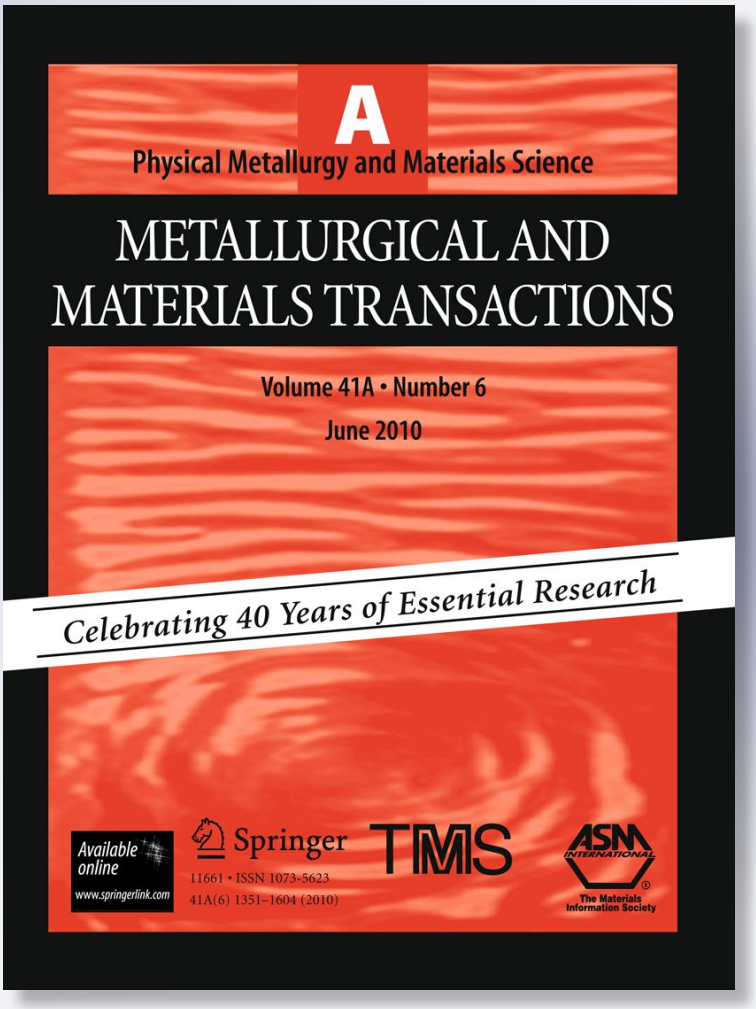

Springer

Your article is protected by copyright and all rights are held exclusively by The Minerals, Metals & Materials Society and ASM International (outside the USA). This e-offprint is for personal use only and shall not be self-archived in electronic repositories. If you wish to self-archive your work, please use the accepted author's version for posting to your own website or your institution's repository. You may further deposit the accepted author's version on a funder's repository at a funder's request, provided it is not made publicly available until 12 months after publication.

Springer

Author's personal copy

In-Situ X-Ray Diffraction Observations of Low-Temperature Ag-Nanoink Sintering and High-Temperature Eutectic Reaction with Copper

JOHN W. ELMER and E.D. SPECHT

Nanoinks, which contain nanometer-sized metallic particles suspended in an organic dispersant fluid, are finding numerous microelectronic applications. One characteristic of nanoinks is that they sinter at much lower temperatures than bulk metals due to their high surface area to volume ratio and small radius of curvature, which reduces their melting points significantly below their bulk values. The unusually low sintering temperatures have unique potential for materials joining, since their melting points increase dramatically afterward. In this article, the sintering kinetics of Ag nanoink is studied using *in-situ* synchrotron methods to determine diffraction peak characteristics during the sintering cycle, and to subsequently calculate particle size and growth during sintering. Ag nanoink is further explored as a eutectic bonding medium by tracking phase transformations between sintered Ag nanoink and a Cu substrate to high temperatures, where melting occurs at the Ag-Cu eutectic, demonstrating nanoinks as a viable eutectic bonding medium.

DOI: 10.1007/s11661-011-0717-9
© The Minerals, Metals & Materials Society and ASM International (outside the USA) 2011

I. INTRODUCTION

NANOINKS are being developed for the direct writing of electrically conductive fine wiring as lower cost alternatives to conventional photolithography.[1,2] The nanosized particles sinter at much lower temperatures than bulk metals due to their high surface area to volume ratio and small radius of curvature.[3] Sintering may be accelerated by local melting as well as by rapid solid-state diffusion. Silver, for example, has a bulk melting temperature of 1235 K (962 °C), but can be made into nanoinks that sinter at temperatures around 473 K (200 °C) for particle sizes less than 20 nm.[2,4] Silver nanopastes (high viscosity) and nanoinks (low viscosity) are available from multiple sources[5] and are being considered for materials joining concepts in addition to microelectronics.[6,7] Nanoinks are further being developed from Cu[8] as a lower cost alternative to more noble Ag and Au,[9] and from Sn-based alloys as lower melting point alternatives for lead-free solder applications.[10]

The unusually low sintering temperatures of nanoparticulate inks and pastes allow them to be used for materials joining, since bonds can be made at low temperatures, but have high melting temperatures after initial sintering.[4,6,7,10] The high melting temperature allows subsequent joints to be made at the same, or even higher, temperatures to facilitate multiple joining sequences and repair work often required in microelectronic packaging. One drawback is that nanoinks require organic surfactants to disperse the nanoparticles and keep them from agglomerating at room temperature.[2] These dispersants need to be removed in order for sintering to take place, and this is usually done by thermal processing. The thermal treatment requires temperatures in excess of 423 K (150 °C) to remove the organic dispersants,[2] which is often performed using bulk heating methods, although flash heating has also been explored.[11]

Improper sintering can result in joints with poor mechanical properties, so understanding the kinetics of sintering is important. In this investigation, silver nanoink is studied using *in-situ* synchrotron-based X-ray diffraction to both follow sintering and to further study the high-temperature behavior of sintered deposits. This work continues similar work by the same authors where silver nanoink was explored as a possible eutectic bonding medium providing a less expensive alternative to physical vapor deposition or electroplating methods.[12] The results presented here track the sintering kinetics of Ag nanoinks in real time as well as eutectic bonding at elevated temperatures. In addition, preliminary mechanical properties of sintered and bonded joints in copper are investigated to determine the effectiveness of Ag nanoinks as bonding mediums.

II. EXPERIMENTAL PROCEDURES

In-situ X-ray diffraction experiments were conducted on Ag nanoink by heating and cooling a Cu substrate coated with the nanoink under controlled conditions

JOHN W. ELMER, Group Leader for Materials Processes, is with the Engineering Technologies Division, Lawrence Livermore National Laboratory, Livermore, CA 94551-0808. Contact e-mail: elmer1@llnl.gov E.D. SPECHT, Member of Technical Staff, is with the Oak Ridge National Laboratory, Oak Ridge, TN, 37831-6118.
Manuscript submitted November 5, 2010.
Article published online May 5, 2011

 U.S. GOVERNMENT WORK NOT PROTECTED BY U.S. COPYRIGHT

Author's personal copy

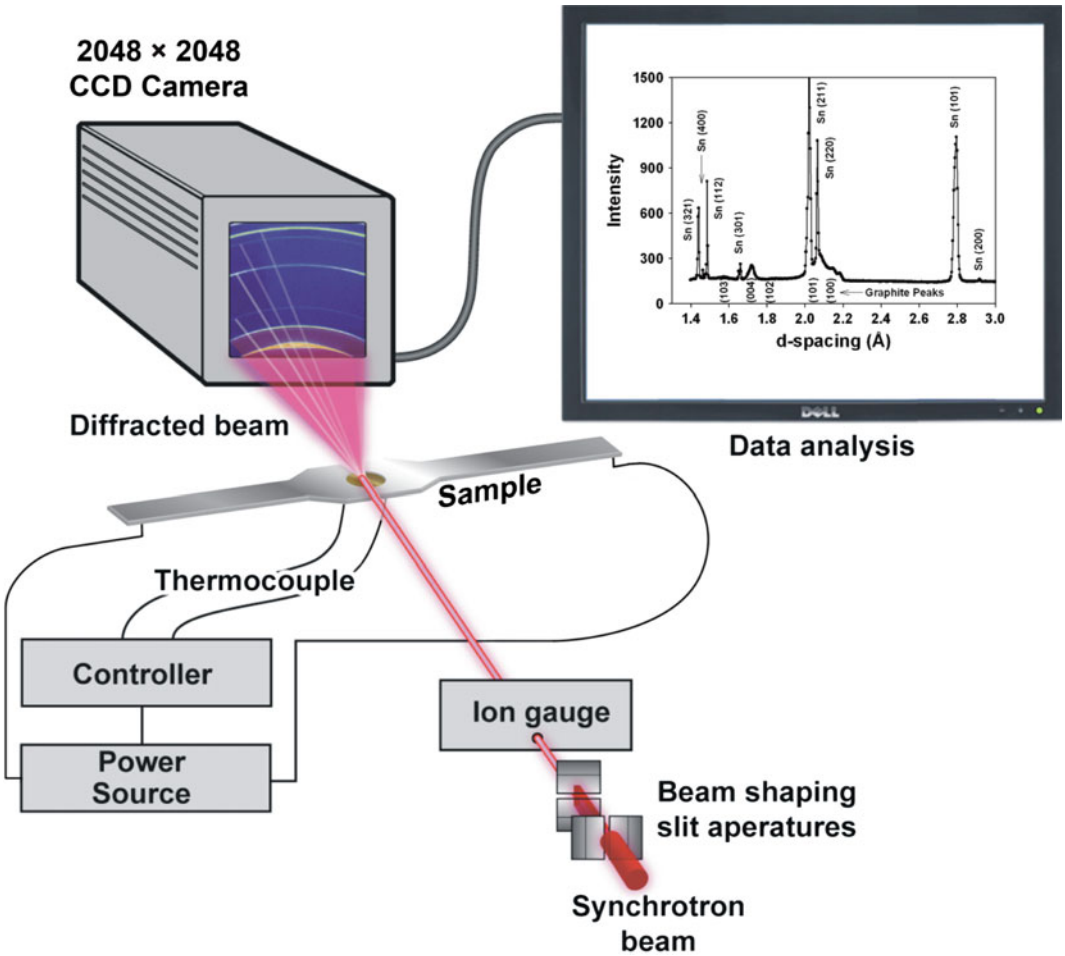

Fig. 1—Schematic of the synchrotron setup showing the basic elements for direct observations of materials being heated resistively in a graphite sample holder. The sample and holder are enclosed in an environmental chamber (not shown) to protect them from oxidation.

while simultaneously performing X-ray diffraction in real time. These experiments were performed at the Advanced Photon Source (APS), using the UNICAT beam-line BM-33-C with X-ray beam energy of 27.9 keV (λ = 0.4476 nm) from a ring current of 100 mA. Figure 1 shows a schematic of the synchrotron X-ray bending-magnet beam line, which is set up with a water-cooled Si (111) monochromator. The monochromatic beam is focused and sized to dimensions of approximately 2-mm wide by 0.5-mm high using a dynamically bent Si crystal and collimator slits. The diffracted beams are detected with a 2048 × 2048 pixel areal detector placed downstream from the sample, and the diffraction patterns are acquired every 2 seconds using a 1-second integration time to provide Debye arcs corresponding to the diffracting planes.

Diffraction patterns were created by integrating the diffraction arcs about their central point to create an intensity *vs* *d*-spacing plot using FIT2D software available from ESRF.[13] Least-squares fitting to Gaussian line shapes was used to determine peak position, intensity, and width. Lattice parameters were found using Bragg's law, where the room-temperature diffraction pattern of the Cu substrate was used as an internal lattice parameter standard. Peak widths were used to determine particle sizes using the Scherrer formula.[14] Additional details about this X-ray beam line and data analysis can be found in References 12,15,16, and 17.

Nanoinks are fluids that require a special experimental setup for *in-situ* observations, and to do this, a graphite heater was designed to indirectly heat a substrate coated with Ag nanoink. A schematic drawing of the sample holder is shown in Figure 2, indicating that the graphite heater measures 100-mm long and 8-mm wide, and has a central portion that allows a 6.3-mm-diameter Cu substrate to be placed inside. The substrate is illustrated in Figure 3, indicating that it has a 5.3-mm-diameter flat surface upon which the nanoink is placed and which is irradiated by the X-ray beam. A blind hole is drilled from the back side of the substrate to allow a 125-μm-diameter type K thermocouple to be placed inside of it. The tip of the thermocouple is approximately 500 μm below the surface of the Cu substrate, minimizing the temperature differential between the nanoink on the surface of the Cu and the temperature measurement location. Silver-loaded thermally conductive epoxy is used to hold the thermocouple in the backside of the substrate, while thermally

Author's personal copy

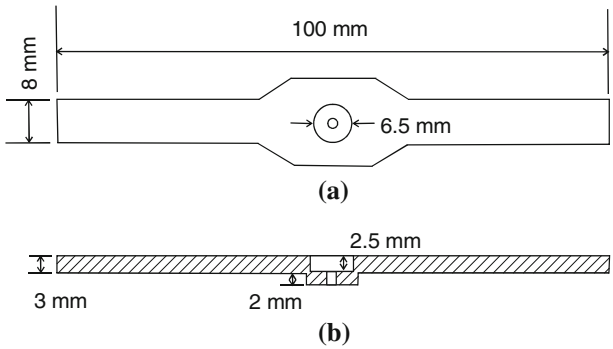

Fig. 2—Graphite heater design: (*a*) top view and (*b*) cross-sectional side view. The circular disk sample is placed in the hole (6.5-mm diameter) in the top center of the heater. A small hole is drilled through the sample holder to allow a thermocouple to be inserted into the sample.

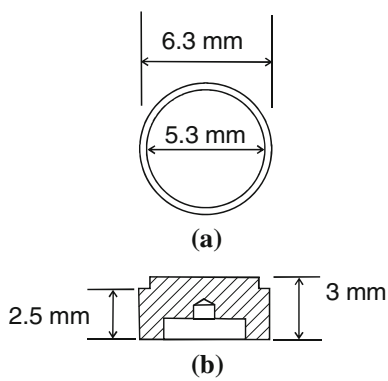

Fig. 3—Schematic drawing of the Cu sample that fits inside the heater shown in Fig. 2. (*a*) Top view showing the 5.3-mm-diameter surface where the Ag nanoink is placed, and (*b*) cross-sectional view showing the thermocouple well.

conductive silver-loaded grease is used on the bottom and sides of the substrate to ensure good thermal contact between the substrate and the graphite heater.

The nanoink used in the experiments was produced by Harima and is designated NPS-J. It is composed of 53 to 58 mass pct Ag in tetradecane, with a reported particle size of 3 to 7 nm, a viscosity of 8.4 mPa·s, and a recommended sintering temperature of 473 K (220 °C). The nanoink was placed on high-purity oxygen-free–high-conductivity Cu substrates using a syringe to apply one drop to the 5.3-mm-diameter Cu substrate, where it quickly wet the surface and formed a meniscus on the top circular surface of the substrate. The thickness of the liquid layer was not measured but was estimated to be about 10- to 15-μm thick. The *in-situ* experiments were performed by placing the Cu sample with the nanoink deposit into a graphite heater, and then placing the heater into the water-cooled grips of the heating stage with a ~5 deg tilt to the axis of the X-ray beam. The Cu substrate was aligned in the graphite heater so that the 2 mm × 0.5 mm X-ray beam was centered on the surface of the Cu sample to observe reactions with the nanoink.

Sintering was performed by first heating the sample in air while simultaneously performing X-ray diffraction to determine the kinetics of the sintering process. Once the sintering was complete, an environmental chamber was placed over the sample holder stage and evacuated to approximately 10 mTorr using a turbo-molecular pump. The Ag-Cu eutectic reaction was then performed in vacuum to prevent oxidation of the sintered silver while heating to high temperatures. *In-situ* X-ray diffraction patterns were collected in real time throughout the experiment and analyzed later to observe the phase transformations that occurred during sintering and heating to elevated temperatures.

Postdiffraction analysis was performed using scanning electron microscopy (SEM) to observe the sintered Ag deposits. In addition, joints were made between copper samples using Ag nanoink sintering and also by high-temperature eutectic bonding. Preliminary mechanical properties of these joints were measured using a shear-testing technique.

III. RESULTS AND DISCUSSION

A. *Ag Nanoink Sintering*

The recommended nanoink sintering profile requires heating in air at 493 K (220 °C) for approximately 60 minutes. This heating cycle is sufficient to burn off the organic dispersants and to subsequently sinter the nanoparticles into a solid layer.[6] Figure 4 shows SEM micrographs of the as-sintered Ag nanoink surface. At low magnifications (Figure 4(a)), the surface contains small ridges that appear light in contrast and are presumed to be caused by nonuniform contraction of the nanoink as the volatile constituents evaporate during sintering. At higher magnifications (Figure 4(b)), the surface is clearly composed of agglomerated particles that are less than 100 nm in diameter. Some porosity is present in the sintered film. The thickness of Ag layer was estimated to be less than 10 μm after sintering. This thin layer of silver allows the high energy synchrotron beam (27.9 keV) to penetrate completely through it and into the Cu substrate below, producing diffraction peaks from both metals during sintering.

In-situ X-ray diffraction was used to follow the sintering kinetics during heating and cooling of the Ag nanoink, and the results at a sintering temperature of 493 K (220 °C) are summarized in Figure 5. The *in-situ* X-ray diffraction patterns are shown on the left in pseudo-color where lighter colors correspond to higher intensity peaks. The diffraction patterns are plotted sequentially from the beginning of heating (t = 0 seconds) to the end of the experiment after cooling (t = 570 seconds). Two diffraction peaks each are present in the d-spacing window of 1.8 to 2.4 Å, representing the fcc (111) and the (200) planes of both Ag and Cu. The corresponding temperature profile is shown on the right-hand side of the figure, indicating that the sample was heated at a rate of 1 K/s and held isothermally at 493 K (220 °C) for 5 minutes prior to being rapidly cooled back to room temperature. In

Author's personal copy

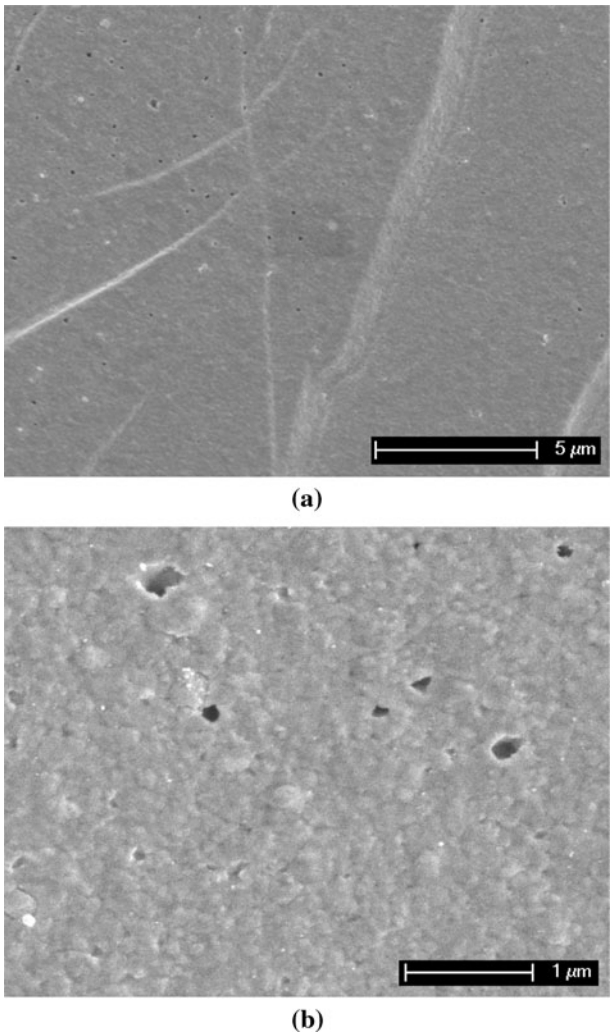

Fig. 4—SEM micrographs of the sintered Ag nanoink surface. (*a*) Low-magnification image showing steps that formed on the surface during sintering. (*b*) Higher magnification image showing sintered particles with diameters less than 100 nm and occasional pores in the sintered film.

addition, the intensity of the Ag (111) peaks was measured using diffraction peak fitting software, and the results were normalized to unity and are plotted in this figure.

The most significant observation of the sintering results is the sharpening of the Ag diffraction peaks, from something very diffuse at low temperatures to sharp peaks that form during the isothermal hold. During this transition, the intensity of the Cu peaks remains relatively constant by comparison. Sintering of the Ag nanoink appears to begin at a temperature of 433 K (160 °C) during the ramp to 493 K (220 °C), as indicated by the dashed lines in Figure 5. At this temperature, the organic dispersants in the nanoink begin to decompose, allowing Ag nanoparticles to come into contact to initiate the sintering process. As the temperature increases, the Ag peak intensity increases by an order of magnitude from a normalized peak intensity of 0.096 (424 counts) to 1.0 (4429 counts) at the end of the thermal cycle. Almost all of the increase in intensity of the diffraction peak occurs during the isothermal hold at 493 K (220 °C), and the trend of the peak intensity with time during the isothermal hold follows a sigmoidal shape. Based on these data, it appears as though a 5-minute hold time at 493 K (220 °C) is sufficient to sinter the NPS-J nanoink into a stable configuration. Additional experiments are planned as future work to determine the kinetics of the sintering process at different holding times and temperatures.

As the diffraction peaks increase in intensity, there is a corresponding decrease in their widths, as shown in Figure 6. The change in width provides important microstructural information about the sintering process. Figure 6(a) plots the FWHM peak width of the Ag(111) planes *vs* time, which is the highest intensity diffraction peak of the silver phase. The peak width is nearly constant for the first 180 seconds of the sintering cycle and then decreases at a decreasing rate until the peak width drops to approximately 0.2 of its initial value. Also plotted in this figure are the particle sizes, as calculated from the Scherrer formula: $D = Kd^2/\mathrm{FWHM}$.[14] In this relationship, the particle size, D, is directly related to the d-spacing of the lattice planes and inversely related to the FWHM of the 2-θ diffraction peak width. Here, we assume equiaxed particle shapes, with a proportionality constant of $K = 0.94$. The initial diffuse peaks are broad with low intensity and correspond to small particle sizes that are calculated to be 9.9 nm. This initial particle size is larger than the reported particle size of 3 to 7 nm, which may be due to partial drying and associated agglomeration of the particles while setting up the *in-situ* diffraction experiments. During heating, the particle size is constant for the first 180 seconds of the sintering cycle, and then increases to approximately 45 nm at the end of the cycle. The particle size, as measured from the (200) planes, was slightly larger at the end of the thermal cycle at 54 nm. The particle size is further plotted in Figure 6(b), but now as a function of sintering temperature rather than time. Here, it is clear that the majority of the increase in particle size occurs during the isothermal hold at 220 °C and that the particle size is nearly constant during subsequent cooling.

B. *Ag Nanoink High-Temperature Eutectic Reaction with Copper*

After sintering, the nanoink deposits are reported to have properties similar to bulk material. For example, electrical resistivity is reported to be within 2 to 3 times the bulk values,[11] and melting temperatures are assumed to be equal to bulk values.[6] Resistivities of the sintered deposits are frequently studied for their use in microelectronics applications and provide some information about sintering; however, demonstration of the high remelt temperature of sintered nanoinks was not performed in detail. In order to verify the high remelt temperature, one of the sintered Ag nanoink deposits on Cu was reheated in vacuum to 1088 K (815 °C) while simultaneously performing *in-situ* X-ray diffraction. The peak temperature is above the Ag-Cu

Author's personal copy

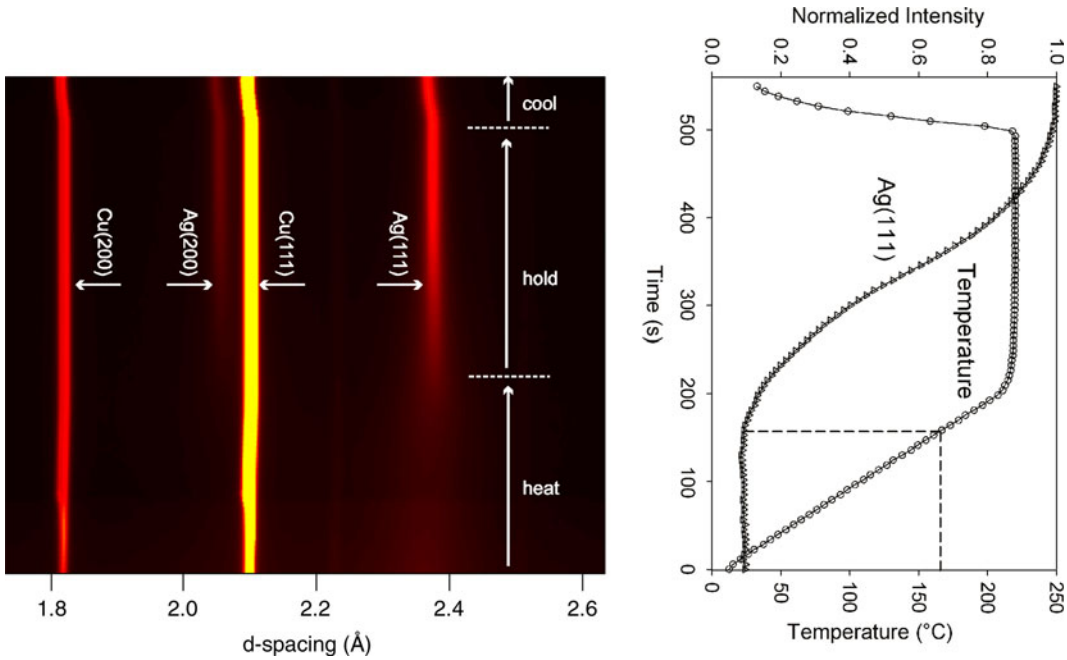

Fig. 5—Thermal cycle for Ag nanoink sintering at 473 K (220 °C). *In-situ* X-ray diffraction patterns are plotted in pseudo-color on the left, with corresponding temperature profile and normalized peak intensity (maximum counts = 4429) plotted for Ag on the right. Sintering begins at a temperature of approximately 433 K (160 °C), as indicated by the dashed line.

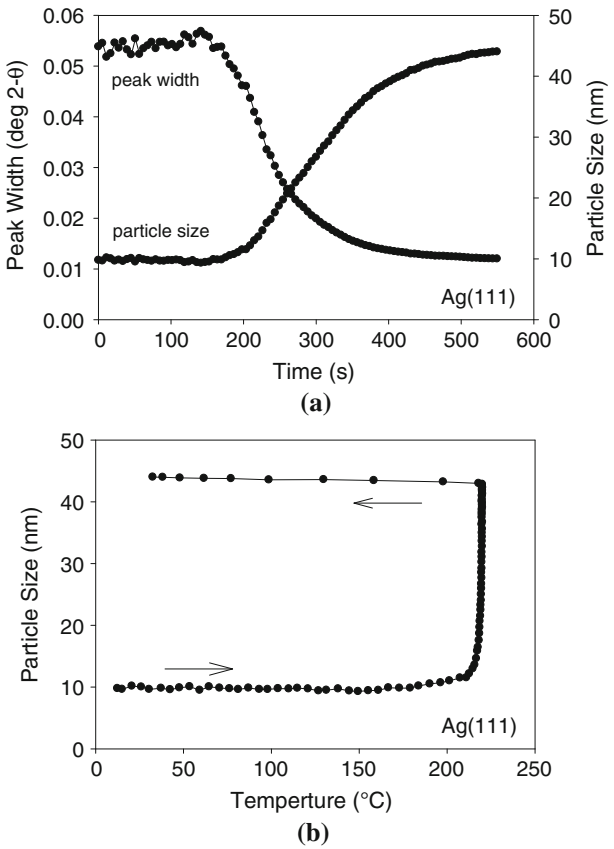

Fig. 6—(*a*) Diffraction peak width of the Ag 111 reflection during sintering and calculated particle size as a function of time. (*b*) Calculated particle size function of temperature, where the arrows indicate heating and cooling.

eutectic temperature of 1053 K (780 °C).[18] If the sintered Ag nanoink melts at this temperature, it would demonstrate both the high-temperature stability of the Ag-sintered deposit and the ability of nanoinks to be used to produce high-temperature eutectic solders or brazes.

The results of the high-temperature reheating experiment are presented in Figure 7, which shows the intensity of the diffraction peaks during heating and cooling. As before, the *in-situ* X-ray diffraction patterns are shown on the left with the diffraction patterns plotted sequentially from the beginning of heating (t = 0 seconds) to the end of the experiment after cooling (t = 730 seconds). The same two diffraction peaks are shown representing the fcc (111) and the (200) planes of Ag and Cu. The right side of the figure shows the corresponding temperature profile, indicating that the sample was rapidly heated at a rate of 10 to 1088 K (815 °C), where it was held for approximately 30 seconds prior to being cooled at a similar rate to room temperature. The intensity of the Ag (111) peaks was measured using diffraction peak fitting software, and the results are also plotted in this figure.

The Ag (111) and Cu (111) diffraction peaks are more intense than the Ag (200) and Cu (200) planes, but otherwise show similar features, so only the (111) planes will be discussed. In the case of Ag, the intensity of the initial normalized diffraction pattern is approximately 0.5 (4429 counts), which is nominally the same value as after the sintering experiment. This value increases to 1.0 (8286 counts) at the end of the remelting experiment. A large fraction of the increase in the Ag (111) peak intensity occurs during heating, and does so only after the temperature passes above the initial sintering

Author's personal copy

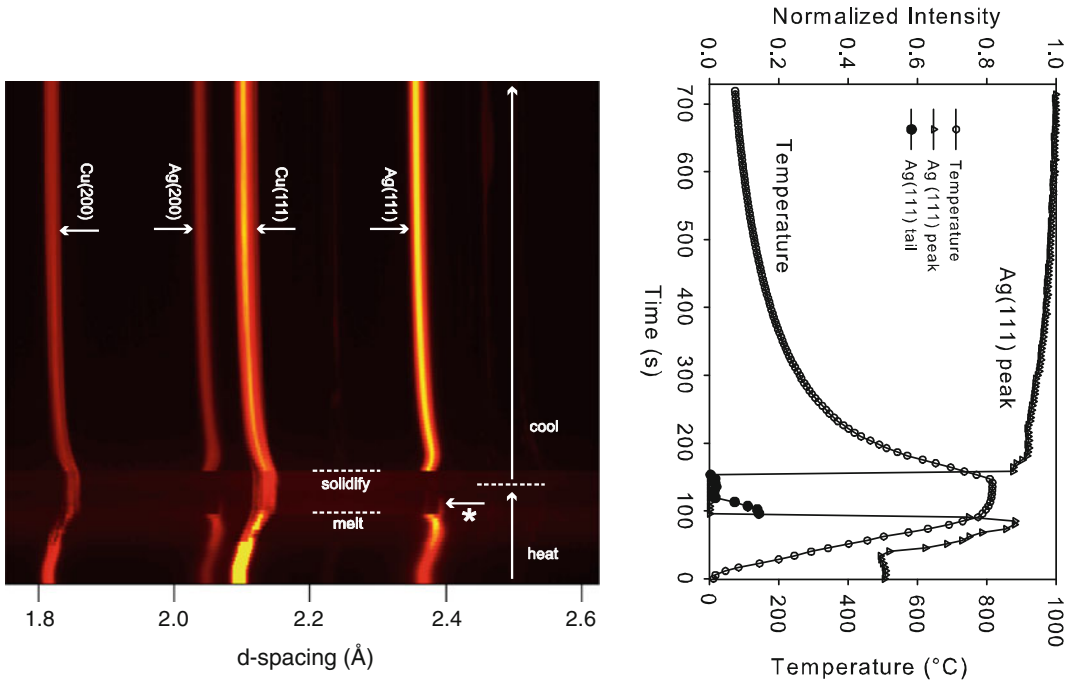

Fig. 7—Reheat cycle of the sintered Ag deposit. *In-situ* X-ray diffraction patterns are plotted in pseudo-color on the left, with the corresponding temperature profile and normalized peak intensity (maximum counts = 8286) plotted for Ag on the right.

temperature of 493 K (220 °C). The increase in the intensity of the Ag (111) peaks results in a rise to 0.75 (6190 counts), which is 1.4 times that after sintering at 493 K (220 °C). This indicates that sintering may not have been completed at 493 K (220 °C) during 5 minutes of hold, and that higher temperatures likely create a more densely sintered Ag layer with larger grain size and stronger diffraction peaks. The Ag peaks are present all the way up to a temperature of 1062 K (789 °C), where a rapid drop in intensity occurs as the main Ag (111) peaks disappear. The disappearance of these peaks indicates that melting does occur, but not until the temperature has reached the Ag/Cu eutectic temperature of 1053 K (780 °C), where Ag and Cu interdiffuse to create the eutectic alloy. Differences between the observed melting temperature of 1062 K (789 °C) and the eutectic of 1053 K (780 °C) can be explained by the time required to react the silver with the copper to form the eutectic composition in an increasing temperature ramp, combined with measurement uncertainties of the thermocouple and the sampling rate.

Careful examination of the diffraction peaks show that not all of the Ag melts at the same temperature. This is indicated by the small peak that tails off of the main Ag (111) peak on the high *d*-spacing side. This tail, indicated by the starred arrow in Figure 7, is most likely the Ag on the top surface of the sample, which is furthest away from the Cu and did not have time to interdiffuse with Cu to create the eutectic composition. The intensity of the Ag (111) peaks in the tail is indicated by the solid circles, and eventually disappears as the sample is held at 1088 K (815 °C). Once power is turned off to the heater, the sample cools at an initial rate of 5 to 10 K/s, and the measured solidification temperature is 1042 K (769 °C). Differences between the observed melting temperature and the eutectic temperature are most likely related to sampling rate uncertainties at the high cooling rate, combined with temperature gradients in the substrate. Accompanying solidification is a rapid increase in the Ag diffraction peaks to a normalized intensity of about 0.6 (7249 counts), which increases to 1.0 (8286 counts) as the sample cools to room temperature.

The results of the reheating experiment clearly show that the sintered Ag nanoink withstands temperatures all the way to the Ag-Cu eutectic temperature of 1053 K (780 °C), which is consistent with the sintered Ag having a bulk melting temperature if it hadn't reacted with the Cu substrate. In addition, the ability of the sintered Ag deposit to react with Cu and melt at the eutectic temperature demonstrates the possibility of using nanoinks as indirect soldering and brazing mediums.

The widths of the Ag diffraction peaks show a distinct increase at high temperatures, which is further indication of the phase transformations that are occurring between Ag and Cu. Figure 8(a) plots one of these results, showing the Ag(111) peak width *vs* temperature for heating to 1088 K (815 °C) and cooling, where the arrows indicate the direction of heating and cooling. On heating, the peak width decreases a small amount during heating above 493 K (220 °C), and this decrease corresponds to the increase in peak intensity at these temperatures, as shown in the previous figure. However, when the temperature approaches the eutectic, there is a rapid increase in the peak width of more than 2 times prior to the eutectic reaction and melting. On cooling, and after solidification of the Ag phase, the peak width returns to its high value, but decreases rapidly back to a

Author's personal copy

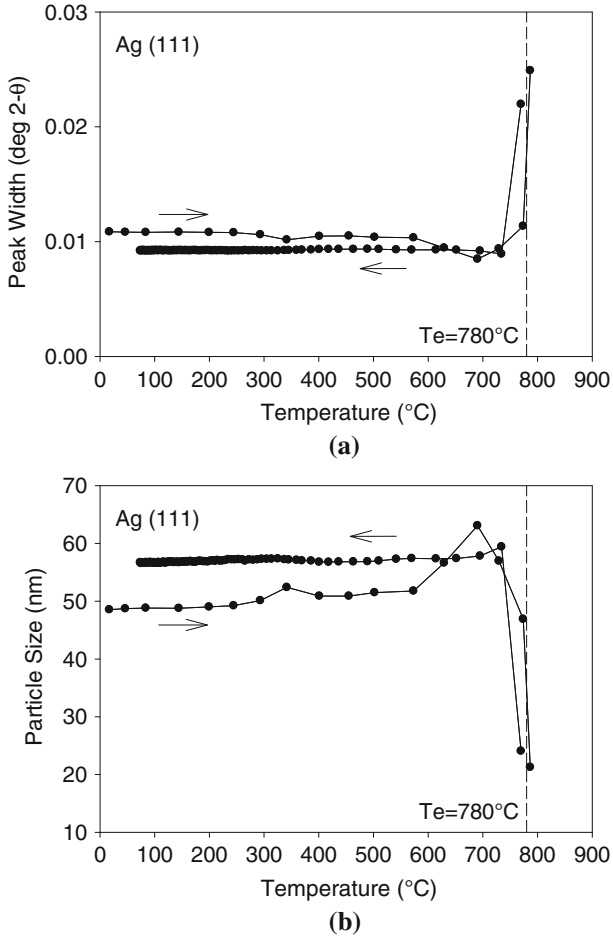

Fig. 8—(*a*) X-ray diffraction peak width and (*b*) calculated particle size of sintered Ag nanoink during heating and cooling to 1088 K (815 °C). Melting occurs at the Ag-Cu eutectic temperature, Te, of 1053 K (780 °C). Arrows indicate the direction of heating and cooling.

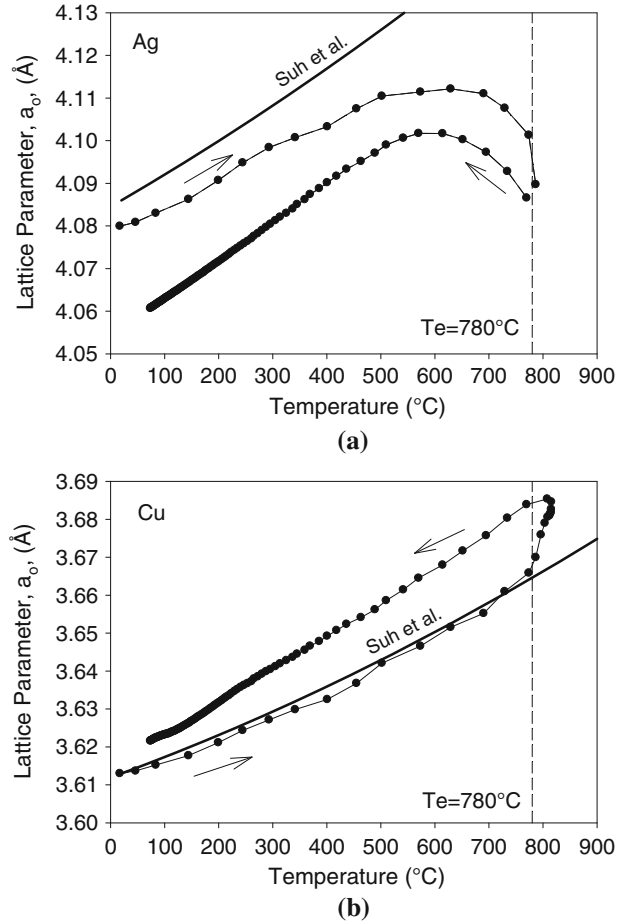

Fig. 9—Lattice parameters based on the (111) peaks of (*a*) sintered Ag nanoink and (*b*) Cu substrate during heating to 1088 K (815 °C) and subsequent cooling. Melting occurs at the Ag-Cu eutectic temperature, Te, of 1053 K (780 °C). Arrows indicate the direction of heating and cooling. Lattice parameter data from Suh *et al.*[20] are superimposed for reference.

width similar to that prior to the remelting cycle. The peak width reaches this value at approximately 973 K (700 °C) on cooling and then remains constant to room temperature. This reversible behavior of the peak width that occurs at high temperatures is not related to further sintering of the Ag layer, since the peak width increases, rather than decreases, with increasing temperature, and is related to the interdiffusion of Ag and Cu, as described subsequently. These same results are plotted in Figure 8(b), as calculated particle size *vs* temperature, showing that the starting size of the sintered particles is 48 nm and grows to 60 nm prior to reacting with copper and melting at 1053 K (780 °C). Upon cooling, the Ag solidifies into a structure that diffracts with a particle size of 58 nm, and this particle size remains during cooling to room temperature.

C. *Lattice Parameters and CTEs During Reheating to High Temperatures*

In-situ diffraction not only provides the intensity and width of the peaks, but it can also be used to determine the lattice spacing as a function of temperature during heating and cooling. This additional information is useful for measuring internal stresses caused by various mechanisms including the interdiffusion of species.[14] In the case of the high-temperature reheating of the Ag nanoink, the diffraction patterns show that the Ag peaks disappear during melting, but the Cu peaks remain throughout the entire experiment. The presence of the Cu peaks indicates that the melt layer is thin enough to allow the X-rays to pass through it and into the underlying solid Cu substrate below. Observations of changes in the lattice parameters of these two phases at elevated temperature provide more detailed information about the high-temperature and eutectic reaction between Ag and Cu.

The results for Ag are presented in Figure 9(a), which plots the lattice parameter, a_o, for Ag based on the (111) planes. During heating, the lattice parameter increases approximately linearly up to a temperature of 773 K (500 °C), where it levels off before decreasing with increasing temperature at 873 K (600 °C). The decrease in the lattice parameter is caused by interdiffusion of Cu

Author's personal copy

Table I. Summary of the CTEs for Sintered Ag and the Cu Substrate on Heating and Cooling for the (111) and (200) Planes, Compared to Reported Bulk Values

	Silver CTE (ppm/K)			Copper CTE (ppm/K)		
Temperature Range [K (°C)]	(111)	(200)	Average	(111)	(200)	Average
298 to 773 (25 to 500) (heating)	15.9	15.8	15.9	17.1	17.2	17.2
773 to 373 (500 to 100) (cooling)	22.1	22.0	22.0	22.3	22.1	22.2
Reported[20,26]	—	—	22.1	—	—	17.5 to 18.5

into the Ag layer and the smaller lattice parameter of Cu (3.608 Å) than Ag (4.086 Å).[19] The Ag peaks reappear on solidification, and the process is reversed, with the lattice parameter increasing during cooling to a temperature of about 873 K (600 °C) and then decreasing after that to room temperature. The nonlinear behavior is related to the higher solubility of Cu in Ag at elevated temperatures, which is reported to be 14 at. pct at 1053 K (780 °C) *vs* less than 0.1 at. pct at room temperature.[18] The decrease in the solubility of Cu with decreasing temperature causes a Cu-rich phase to separate from the Ag-Cu alloy during cooling, which results in an increase in the lattice parameter of the remaining Ag. The separation of Cu from Ag requires thermally activated diffusion to take place, which is not sustained at temperatures below about 773 K (500 °C) for the cooling rate of 10 K/s, resulting in typical contraction behavior of the Ag-rich phase at lower temperatures. A net decrease in the Ag lattice parameter of 0.02 Å, from 4.08 to 4.06 Å, occurs during the reheating and cooling cycle due to the remnant Cu in the Ag film. Also plotted in Figure 9(a) is the lattice expansion curve for pure Ag, as determined by high-temperature X-ray diffraction.[20] The expansion curve shows a slight nonlinear behavior that has an increasing slope with increasing temperature. These data deviate strongly from the sintered Ag on the Cu substrate at temperatures above 773 K (500 °C), as expected, since the pure material will expand without the effects of chemical interdiffusion. An additional point is that the initial lattice parameter of the sintered Ag of 4.08 Å is 0.005 Å lower than the reported value,[20] which is most likely due to the effect of surface stresses on small particles, which is known to decrease the lattice spacing.[21]

The lattice parameter for Cu is plotted in Figure 9(b) for comparison, showing a strong deviation from its low-temperature expansion trend for temperatures above 1053 K (780 °C) when Cu is in contact with the liquid Ag-Cu eutectic alloy. In this case, the lattice parameter increases rapidly at high temperatures rather than decreasing like Ag. During cooling, the lattice parameter of the Cu phase decreases in a nearly linear manner. There is a small net increase in the lattice parameter of Cu of 0.009 Å after cooling back to room temperature due to interdiffusion of Ag into the Cu substrate. Also plotted in Figure 9(b) is the lattice expansion curve for pure Cu, as determined by high-temperature X-ray diffraction.[20] This curve shows a slight nonlinear behavior that has an increasing slope with increasing temperature and matches the measured expansion of Cu beneath the sintered Ag reasonably well up until the point where Ag melts and reacts with the Cu substrate.

The lattice parameter data presented in Figure 9 were used to determine the coefficient of thermal expansion (CTE) of the sintered Ag deposit and the Cu substrate. This was done for both the heating and cooling cycles, for the (111) and (200) planes. The results are summarized in Table I for a temperature range of 298 to 773 K (25 to 500 °C), which is the range where interdiffusion of Ag and Cu appear to be negligible. The measured average CTE of Ag on heating was similar for both planes and had an average value of 15.9 ppm/K. This is considerably less than the measured average CTE on cooling of 22.0 ppm/K. The reported CTE of bulk Ag is 22.1 ppm/K over this temperature range,[22] is close to the measured value on cooling, but deviates considerably from the measured CTE of the sintered Ag during heating. The low CTE measured on heating is most likely due to the Ag sintered film not being fully dense. Lattice expansion was reported for nanocrystalline Cu, Nb, and Ni, relative to microcrystalline or single-crystal values, attributed to either surface tension, expanded grain boundaries, or vacancies.[23–25] If a similar effect occurs in Ag, a lattice contraction would occur as grains grow with increasing temperature, accounting for the reduced CTE.

The same CTE measurements were made on Cu for both the Cu(111) and Cu(200) planes, and the results are also summarized in Table I and compared to data for bulk materials from the open literature. The measured average CTE for Cu over the 298 to 773 K (25 to 500 °C) temperature range is 17.2 ppm/K, whereas on cooling, the average CTE was 22.2 ppm/K. The CTE on heating is very close to the high-temperature X-ray data provided by Suh *et al.*[20] and is slightly higher than the reported CTE for bulk Cu over this same temperature range of 18.5 ppm/K.[26] The higher measured CTE of Cu on cooling than bulk Cu is caused by diffusion of the higher CTE Ag into the Cu base metal substrate.

D. *Mechanical Properties of Sintered and Eutectic Bonded Joints*

Preliminary bonding experiments were performed using Ag nanoink to join together two copper coupons on their 5.3-mm-diameter surfaces (Figure 3). Each surface was first coated with one drop of the Ag nanoink, and then they were then placed together prior to sintering at 493 K (220 °C) for 15 minutes in air. After sintering, some of the samples were brazed by

Author's personal copy

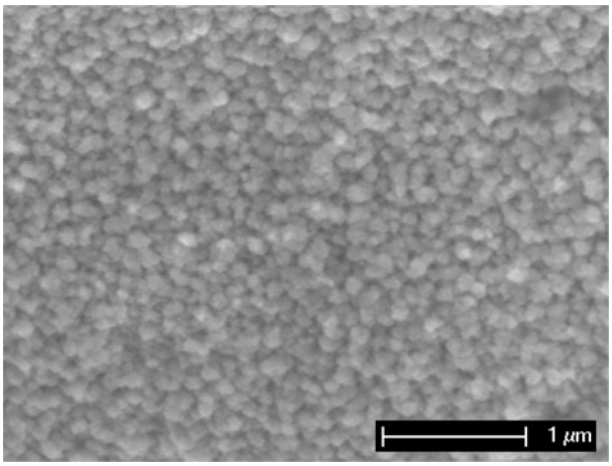

Fig. 10—SEM micrograph of the edge of the fracture surface of the sintered Ag nanoink joint on copper, showing sintered particles having diameters less than 100 nm.

heating to 1088 K (815 °C) in a vacuum furnace to form a eutectic bond between the sintered Ag layer and the copper so that the properties could be compared to the as-sintered bonds in Cu.

Mechanical testing was performed by clamping one side of the joined copper piece in a V-block assembly and shearing the mating part at a constant displacement rate of 2 μm/s in a screw-driven tensile testing machine. Due to the nonstandard nature of the test coupons, only the peak load at failure is reported, as some slippage in the grips occurred. Two as-sintered coupons were tested and broke at a shear stress (load/bond area) of 0.44 and 0.51 MPa, respectively, which is more than an order of magnitude less than expected for high-quality Ag nanoink joints.[6,7] The reason for the low fracture stress is most likely a combination of factors, including the fact that no load was applied to the joints during sintering and that the sintering temperature was on the low side to produce high-strength bonds. This low fracture stress points out the importance of optimizing and controlling the nanoink sintering parameters in order to produce high-quality joints. Figure 10 is an SEM micrograph of the fracture surface that shows that it is composed of an aggregate of individual sintered particles with diameters less than 100 nm. The size of the particles on the fracture surface is consistent with the particle size estimated from the X-ray diffraction peak widths of 45 nm at the end of the sintering cycle.

The sintered Ag nanoink coupons that were subsequently brazed showed drastically improved properties. Testing of these coupons in excess of 10 MPa was unable to shear the samples apart, and the test fixture was not able to support the samples to higher loads. Subsequent impact testing was performed, which highly deformed the ends of the copper coupon, and yet the braze joint never failed. These results show that the brazed coupons have significantly higher strength than the as-sintered coupons. Full-strength Ag-brazed copper joints are known to have ultimate tensile strengths on the order of 180 MPa,[27] and future work is planned to redesign the mechanical test coupons to a ram-tensile configuration so that more accurate mechanical property information can be obtained on both the as-sintered and brazed joints.

IV. CONCLUSIONS

1. Synchrotron-based X-ray diffraction was demonstrated to be useful for studying real time sintering kinetics of nanoinks and the subsequent phase transformations that occur between them and corresponding substrates.
2. *In-situ* X-ray diffraction performed on Ag nanoink showed that the sintering/curing behavior follows a sigmoidal relationship that nears completion after 5 minutes at 493 K (220 °C).
3. *In-situ* X-ray diffraction performed during reheating of a sintered Ag deposit on Cu showed that the Ag continues to sinter at temperatures above the initial curing temperature of 493 K (220 °C). High-temperature reheating experiments showed that the sintered Ag does not melt until the eutectic phase formed between Ag and Cu at 1053 K (780 °C).
4. *In-situ* particle size estimations of the nanoink were made during sintering using the diffraction peak widths and the Scherrer formula. The results showed that the initial nanoink particle size increases from 9.9 to 45 nm during sintering at 493 K (220 °C). Additional increases in the particle size were observed during reheating to elevated temperatures, reaching 60 nm prior to reacting with Cu and melting at the eutectic temperature of 1053 K (780 °C).
5. *In-situ* measurements of the lattice parameter of the Ag sintered deposit revealed a CTE on heating of 15.9 ppm/K up to 773 K (500 °C), which is considerably lower than the bulk value of 22.1 ppm/K. This difference is presumed to be due to the low density, expanded grain boundaries, or vacancies present in the sintered layer.
6. Above 773 K (500 °C), the lattice expansion of the Ag sintered deposit decreases and becomes negative at temperatures above 873 K (600 °C). This behavior reverses on cooling and is attributed to interdiffusion and the high solubility of Cu in Ag at elevated temperatures.
7. Reaction and melting of the sintered Ag layer with the Cu substrate at 1053 K (780 °C) demonstrates that Ag nanoinks can be used as a eutectic bonding medium.
8. The mechanical properties of Ag nanoink joints in Cu revealed much stronger joints in the eutectic bonded condition as compared to the sintered condition. Future work is planned to better quantify these properties.

ACKNOWLEDGMENTS

The authors thank Jenia Karapetrova, APS, for assisting with the synchrotron beam-line setup and operation. This work was performed under the

Author's personal copy

auspices of the United States Department of Energy (U.S. DOE) by the Lawrence Livermore National Laboratory, under Contract No. DE-AC52-07NA27344, and by the Oak Ridge National Laboratory, under Contract No. DE-AC05-00OR22725. The ORNL portion of this work was fully supported by the Materials Sciences and Engineering Division, Office of Basic Energy Sciences, U.S. DOE. The *in-situ* synchrotron experiments were performed on 34-BM-C at the APS, which is supported by the U.S. DOE, Basic Energy Sciences, Office of Science, under Contract No. W-31-109-ENG-38.

REFERENCES

1. W. Peng, V. Hurskainen, S. Dunford, S. Quander, and R. Vatanparast: *55th Electronic Components and Technology Conference*, May 31–Jun 04, Lake Buena Vista, FL, IEEE, 2005, pp. 77–82.
2. D. Wakuda, K.-S. Kim, and K. Suganuma: *IEEE Trans. Compon. Packag. Technol.*, 2009, vol. 32 (3), pp. 627–32.
3. P. Buffat and J.-P. Borel: *Phys. Rev. A*, 1976, vol. 13 (6), p. 2287.
4. M. Maruyama, R. Matsubayashi, H. Iwakuro, S. Isoda, and T. Komatsu: *Appl. Phys. A*, 2008, vol. 93, pp. 467–70.
5. A. Suzuki, Y. Hasegawa, Y. Ishikawa, T. Komine, H. Morita, and H. Shirai: *Rev. Sci. Instrum.*, 2005, vol. 76, 5 pp.
6. A. Hirose and K.F. Kobayashi: in *Microjoining and Nanojoining*, Y.N. Zou, ed., Woodhead Publishing, Cambridge, UK, 2008, pp. 250–68.
7. A. Hu, J.Y. Gao, H. Alarifi, G. Patene, Y. Zhou, G. Compagnini, and C.X. Xu: *Appl. Phys. Lett.*, 2010, vol. 97, p. 153117.
8. S. Jeong, K. Woo, D. Kim, S. Lim, J.S. Kim, H. Shin, Y. Xia, and J. Moon: *Adv. Functional Mater.*, 2008, vol. 18, pp. 679–86.
9. T. Bakhisheva and V. Subramanian: *J. Electron. Mater.*, 2009, vol. 38 (12), p. 2720.
10. C. Anderson, C. Zou, B. Yang, Y. Gao, J. Liu, and Q. Zhai: *IEEE 2nd Electronics Systemintegration Technology Conf.*, Greenwich, United Kingdom, 2008, p. 915.
11. H.-S. Kim, S.R. Dhage, D.-E. Shim, and H.T. Hahn: *Appl. Phys. A*, 2009, vol. 97, pp. 791–98.
12. J.W. Elmer and E.D. Specht: *Scripta Mater.*, 2010, vol. 63, pp. 1224–27.
13. P. Hammersley, S.O. Svensson, M. Hanfland, A.N. Fitch, and D. Häusermann: *High Press. Res.*, 1996, vol. 14, pp. 235–48.
14. *Elements of X-Ray Diffraction*, 3rd ed., B.D. Cullity and S.R. Stock, eds., Prentice Hall, Upper Saddle River, NJ, 2001.
15. J.W. Elmer, E.D. Specht, and M. Kumar: *J. Elec. Mater.*, 2010, vol. 39 (3), pp. 273–82.
16. J.W. Elmer, T.A. Palmer, and E.D. Specht: *J. Vacuum Sci. Technol.-A*, 2006, vol. 24 (4), pp. 978–87.
17. J.W. Elmer and E.D. Specht: *J. Electron. Mater.*, 2011, vol. 40 (2), pp. 201–12.
18. *Binary Alloy Phase Diagrams*, 2nd ed., ASM INTERNATIONAL, Materials Park, OH, 1990, vol. 2.
19. *Pearson's Handbook of Crystallographic Data for Intermetallic Phases*, Desk ed., ASM INTERNATIONAL, Metals Park, OH, 1997, vol. 2.
20. I.-K. Suh, H. Ohata, and Y. Waseda: *J. Mater. Sci.*, 1988, vol. 23, pp. 757–60.
21. P.A. Montano, W. Schultz, B. Tesche, G.K. Shenoy, and T.I. Morrison: *Phys. Rev. B*, 1984, vol. 30 (2), pp. 672–77.
22. *ASM Metals Handbook*, 9th ed., ASM INTERNATIONAL, Metals Park, OH, 1979, vol. 2.
23. R. Banerjee, E.A. Sperling, G.B. Thompson, H.L. Fraser, S. Bose, and P. Ayyub: *Appl. Phys. Lett.*, 2003, vol. 82 (24), pp. 4250–52.
24. Y. Champion, F. Bernard, N. Millot, and P. Perriat: *Appl. Phys. Lett.*, 2005, vol. (23), p. 1947887.
25. M.Y. Gamarnik: *Phys. Status Solidi B-Basic Res.*, 1991, vol. 168 (2), pp. 389–95.
26. R.E. Taylor: *Thermal Expansion of Solids*, CINDAS Data Series on Material Properties, C.Y. Ho, ed., ASM INTERNATIONAL, Metals Park, OH, 1998, vol. 1–4.
27. J.W. Elmer, J. Klingmann, and K. Van Bibber: *Phys. Rev. Spec. Top. Accel. Beams*, 2001, vol. 4 (5), pp. 53502-1–53502-16.